



Universiteit
Leiden
The Netherlands

Identification and functional analysis of two new de novo KCNMA1 variants associated with Liang-Wang syndrome

Liang, L.N.; Liu, H.H.; Bartholdi, D.; Haeringen, A. van; Fernandez-Jaen, A.; Peeters, E.E.A.; ... ; Wang, Q.K.



Citation

Liang, L. N., Liu, H. H., Bartholdi, D., Haeringen, A. van, Fernandez-Jaen, A., Peeters, E. E. A., ... Wang, Q. K. (2022). Identification and functional analysis of two new de novo KCNMA1 variants associated with Liang-Wang syndrome. *Acta Physiologica*, 235(1). doi:10.1111/apha.13800

Version: Publisher's Version
License: [Leiden University Non-exclusive license](#)
Downloaded from: <https://hdl.handle.net/1887/3561450>

Note: To cite this publication please use the final published version (if applicable).

Identification and functional analysis of two new de novo *KCNMA1* variants associated with Liang–Wang syndrome

Lina Liang¹  | Huihui Liu¹ | Deborah Bartholdi² | Arie van Haeringen³ | Alberto Fernandez-Jaén⁴ | Els E. A. Peeters⁵ | Hongbo Xiong¹ | Xuemei Bai¹ | Chengqi Xu¹ | Tie Ke¹ | Qing K. Wang¹ 

¹Center for Human Genome Research, Key Laboratory of Molecular Biophysics of the Ministry of Education, College of Life Science and Technology, Huazhong University of Science and Technology, Wuhan, P. R. China

²Department of Human Genetics, Inselspital, University Hospital Bern, Bern, Switzerland

³Department of Clinical Genetics, Leiden University Medical Center, Leiden, the Netherlands

⁴Hospital Universitario Quirónsalud, School of Medicine, Universidad Europea de Madrid, Madrid, Spain

⁵Department of Child Neurology, Juliana Children's Hospital, HAGA Medical Center, The Hague, the Netherlands

Correspondence

Qing K. Wang and Tie Ke, Center for Human Genome Research and College of Life Science and Technology, Huazhong University of Science and Technology, 1037 Luoyu Road, Wuhan, P. R. China.

Email: qingwang118@qq.com (Q. K. W) and ket@hust.edu.cn (T. K.)

Funding information

This study was supported by the National Natural Science Foundation of China grants 81970207 and 81630002

Abstract

Aim: Loss-of-function *KCNMA1* variants cause Liang–Wang syndrome (MIM #618729), a newly identified multiple malformation syndrome with a broad spectrum of developmental and neurological phenotypes. However, the full spectrum of clinical features and underlying pathogenic mechanisms need full elucidation.

Methods: Exome sequencing was used to identify pathogenic variants. Patch-clamp recordings were performed to access the effects of *KCNMA1* variants on BK channels. Total and membrane protein expression levels of BK channels were characterized using Western blotting.

Results: We report identification and functional characterization of two new de novo loss-of-function *KCNMA1* variants p.(A172T) and p.(A314T) with characteristics of Liang–Wang syndrome. Variant p.(A172T) is associated with developmental delay, cognitive impairment and ataxia. Mechanistically, p.(A172T) abolishes BK potassium current, inhibits Mg²⁺-dependent gating, but shifts conductance-voltage (G-V) curves to more positive potentials when complexed with WT channels. Variant p.(A314T) is associated with developmental delay, intellectual disability, cognitive impairment, mild ataxia and generalized epilepsy; suppresses BK current amplitude; and shifts G-V curves to more positive potentials when expressed with WT channels. In addition, two new patients with previously reported gain-of-function variants p.(N536H) and p.(N995S) are found to show epilepsy and paroxysmal dyskinesia as reported previously, but also exhibit additional symptoms of cognitive impairment and dysmorphic features. Furthermore, variants p.(A314T) and p.(N536H) reduced total and membrane levels of BK proteins.

Conclusion: Our findings identified two new loss-of-function mutations of *KCNMA1* associated with Liang–Wang syndrome, expanded the spectrum of clinical features associated with gain-of-function *KCNMA1* variants and emphasized the overlapping features shared by gain-of-function and loss-of-function mutations.

Lina Liang and Huihui Liu contributed equally to this work.

KEYWORDS

BK channel, genotype–phenotype correlation, *KCNMA1*, Liang–Wang syndrome, mutation, neurodevelopmental disorder, pathogenic variant

1 | INTRODUCTION

KCNMA1 encodes the α -subunit of the high conductance and calcium-activated BK channel (also known as *KCa1.1*), which plays essential roles in multiple physiological processes, including the regulation of neuronal excitability, neurotransmitter release, smooth muscle contraction, action potential repolarization and cochlear hair cell tuning.^{1–5} Structurally, BK channels are assembled by four α -subunits.⁶ Each α -subunit is comprised of an N-terminal extracellular region (transmembrane segments S0–S1), a voltage sensing domain (VDS, S4) that is coupled to the K^+ channel pore domain and acts as the voltage sensor for channel opening, a pore-forming domain between S5 and S6 for K^+ selective passage⁷ and a large cytoplasmic C-terminal region that is responsible for Ca^{2+} sensing.^{8–10}

Genetic studies enabled the investigation of the roles of *KCNMA1* in different physiological and pathological conditions. In 2005, our laboratory reported the first heterozygous *KCNMA1* mutation p.(D434G), which is a gain-of-function (GOF) mutation leading to an increase in Ca^{2+} sensitivity and voltage-dependent activation of BK channels.¹¹ Mutation p.(D434G) was identified in a large family with generalized epilepsy and paroxysmal dyskinesia induced by enhanced neuronal excitability through the promotion of faster repolarization of action potentials.¹¹ Subsequently, we reported a de novo heterozygous GOF *KCNMA1* variant p.(N995S) in two independent patients with epilepsy.¹² Of note, variant p.(N995S) promoted voltage-dependent activation rather than enhancing Ca^{2+} activation of BK channels.¹² Interestingly, in 2019, we reported eight heterozygous genetic variants of *KCNMA1* in nine unrelated families that inhibited the activity of BK channels, and were defined as loss-of-function (LOF) variants, including p.(S351Y), p.(G356R), p.(G375R), p.(C413Y), p.(N449fs), p.(I663V), p.(P805L) and p.(D984N).¹³ Six of the eight variants occurred de novo in eight families, and one de novo variant, p.(G375R) was identified in three unrelated families.¹³ In contrast to the previously reported GOF variants, the LOF variants of *KCNMA1* were associated with a new multiple malformation syndrome with a broad spectrum of developmental and neurological disorders. This new syndrome was named as Liang–Wang syndrome (LIWAS) by Online Mendelian Inheritance in Man (OMIM) on 7 January 2020.¹³ Liang–Wang syndrome (MIM #618729) was described as ‘a polymalformation syndrome apparent

from birth, which shows large phenotypic variability and severity’ (<https://www.omim.org/entry/618729>). All nine affected patients in our previous report suffered from varying degrees of neurological dysfunction, such as developmental delay and intellectual disabilities with speech delay, strabismus and/or ataxia.¹³ However, the clinical features had a larger variability with regard to ataxia, tremor, epilepsy, dysmorphism and developmental and other features.¹³ Moreover, our study¹³ and another recent study by Mameli et al¹⁴ suggest that type I diabetes may be another clinical feature of Liang–Wang syndrome. Interestingly, homozygous *KCNMA1* variants were also reported, for example, p.(Y676Lfs*7) detected in two siblings with epilepsy, developmental delay and severe cerebellar atrophy, and p.(R458Ter) identified in a patient with paroxysmal dyskinesia, epilepsy, intellectual delay and corticospinal-cerebellar tract atrophy.^{15,16} To date, 19 pathogenic *KCNMA1* variants have been reported to be associated with different neurological disorders in 42 patients.^{14,17–20} Three of them acted by GOF, nine by LOF and three without functional characterization. Moreover, three *KCNMA1* variants were identified in patients, but functional studies suggest that they are benign polymorphism that have no direct cause–consequence relationship with the disease. Almost all of the identified genetic variants are clustered around the pore-forming S5–S6 segments and in the Ca^{2+} sensing C-terminus.^{17,18,20}

In this study, we report four new patients with four different *KCNMA1* variants, including two new de novo variants p.(A172T) and p.(A314T), and two previously reported variants of p.(N536H), and p.(N995S). We carefully characterized these variants by studying their functional effects on electrophysiological and biochemical characteristics of BK channels, and the spectrum of their associated clinical features (ie, genotype–phenotype correlation of the four variants).

2 | RESULTS

2.1 | Identification of four new patients carrying *KCNMA1* variants

Four patients with *KCNMA1* variants were referred to our laboratory for consultation of functionality by genetic counselors, medical/clinical geneticists and physicians. The variants include p.(A172T) located between

transmembrane segment S0 and S1 of BK channels, p.(A314T) in the S5 segment, p.(N536H) in the RCK1 domain and p.(N995S) in the RCK2 domain (Figure 1). Based on the guidelines of the American College of Medical Genetics and Genomics (ACMG),²¹ all four *KCNMA1* variants can be classified as the ‘strong pathogenic’ or PS variants (Table 1).

2.2 | A de novo variant p.(A172T) in the S0-S1 loop abolishes the function of BK channels and decreases Mg²⁺-dependent activation

We identified a heterozygous c.514G>A [p.(A172T)] variant of *KCNMA1* (GenBank accession number NM_002247.3) in a 9-year-old male patient with a history of global developmental delay, borderline cognitive impairment, and ataxia but without paroxysmal dyskinesia, seizures or dysmorphic features (Figures 1 and 2A and Table 2). Variant p.(A172T) was predicted to be deleterious using *in silico* prediction models (Mutation Taster; PolyPhen-2; SIFT). This missense variant was not found in the DNA sequences of his parents, which indicated that this variant occurred de novo (Figure 2A). Alanine 172 is located in the loop between S0 and S1 of BK channels (Figure 1), and the amino acid residue is highly conserved among different species during evolution (Figure 2B). To determine whether variant p.(A172T) affects BK channel

activity, a patch-clamp study was performed in HEK293T cells transfected with expression plasmids carrying either wild-type (WT) or variant *KCNMA1*. Results showed that the cells overexpressing WT *KCNMA1* elicited significant K⁺ current under the voltage stimulus from -160 mV to 160 mV at a Ca²⁺ concentration of 10 μM, whereas the cells overexpressing mutant *KCNMA1* with p.(A172T) failed to elicit any current (Figure 2C). Based on the patch-clamp data, the p.(A172T) variant is a LOF variant.

As the patient harboured a heterozygous variant in the *KCNMA1* gene, we also transfected HEK293T cells with the same amount of both WT (0.5 μg) and variant plasmids (0.5 μg), WT plasmid alone (1.0 μg) or mutant plasmid alone (1.0 μg) to explore whether the p.(A172T) variant acted by a dominant-negative mechanism or a loss of function mechanism. We found that compared with WT channels, WT plus variant BK channels shifted the G-V curve towards a more positive potential by +32 mV at 10 μM Ca²⁺ ($P < .001$) (Figure 2D). We also analysed the normalized amplitude of BK currents at several membrane voltages from a patch of cell membranes to quantify changes in BK currents density. As shown in Figure 2E, the BK current density for the heterozygous WT/mutant channels was about 50% of that of WT channels, which does not support a dominant negative mechanism. However, a caution is needed when interpreting the data because there is no linear correlation between the amount of DNA used for transfection and current densities (Figure S1).

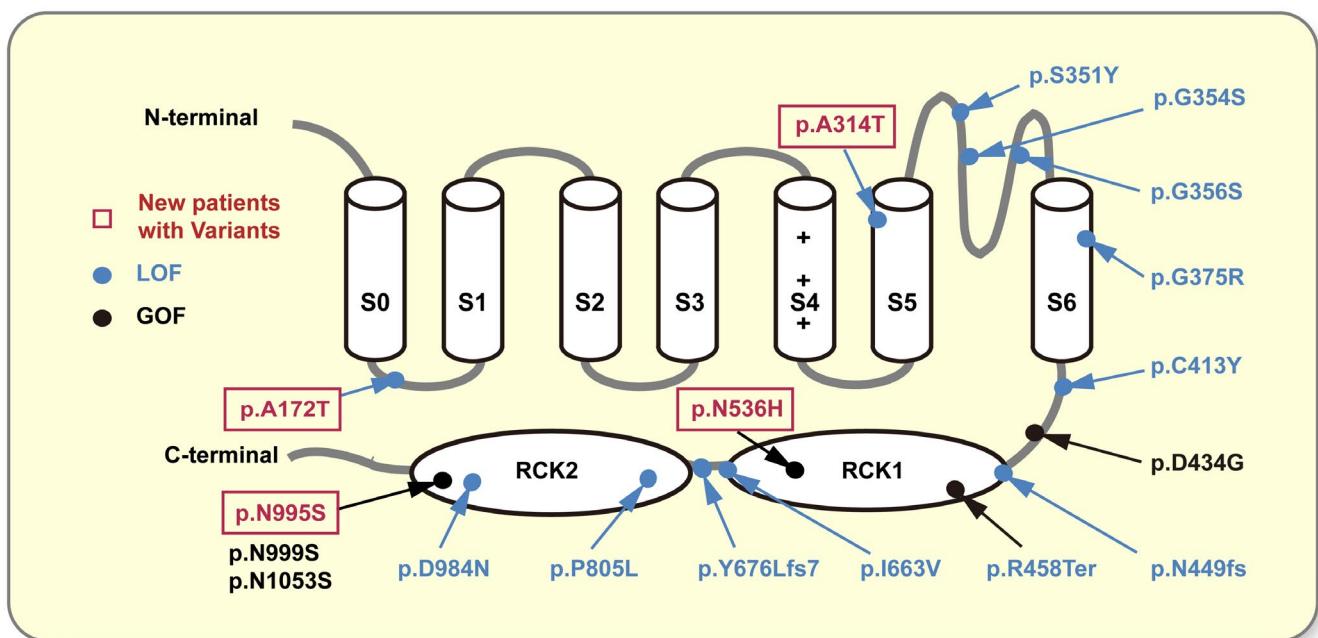


FIGURE 1 A schematic diagram of the BK channel with the location of four pathogenic variants indicated. Variants p.(A172T), p.(A314T), p.(N536H) and p.(N995S) were located in the intracellular loop between S0 and S1 segments, the S5 transmembrane segment, the RCK1 domain and the RCK2 domain, respectively

Gene	Mutation	Type	Category	ACMG standard
<i>KCNMA1</i>	c.G514A, p.A172T	Missense	PS2, PS3, PM2, PP3	PS
<i>KCNMA1</i>	c.G940A, p.A314T	Missense	PS2, PS3, PM1, PM2, PP3	PS
<i>KCNMA1</i>	c.A1606C, p.N536H	Missense	PS2, PS3, PM1, PM2, PP3	PS
<i>KCNMA1</i>	c.A2984G, p.N995S	Missense	PS2, PS3, PM1, PM2, PP3	PS

TABLE 1 Classification of *KCNMA1* variants following ACMG guidelines

Note: PS2, de novo; PS3, well-established in vitro or in vivo functional studies supportive of a damaging effect on the gene or gene product; PM1, located in a mutational hot spot and/or critical and well-established functional domain; PM2, absent from controls (or at extremely low frequency if recessive) in databases; PP3, multiple lines of computational evidence support a deleterious effect on the gene or gene product; PS, pathogenic strong.

We determined whether the heterozygous WT/mutant channels showed calcium-dependent sensitivity to channel activation. Compared with WT channels, cells with co-expressed WT and mutant channels produced more positive G-V curve shift by +22 mV at 0 μ M, +30 mV at 1 μ M and +32 mV at 10 μ M Ca^{2+} ($P < .001$, Figure 2F-H and Table 3). The $\Delta V_{1/2}$ values ($V_{1/2}(\text{p.A172T/WT}) - V_{1/2}(\text{WT})$) were similar at the three different calcium concentrations (Figure 2H). Therefore, the p.(A172T) variant had a minimal effect on the Ca^{2+} -dependent activation of the BK channels.

The S1-S0 loop contains a Mg^{2+} binding site (Asp¹⁶⁴), which contributes to Mg^{2+} modulation of BK channels.²² We hypothesized that the p.(A172T) variant affected the properties of BK channels due to altered Mg^{2+} -dependent gating. To test this hypothesis, we detected the combined effect of WT plus mutant *KCNMA1* on BK channel activation at 0 and 10 mM of intracellular Mg^{2+} . The G-V curves of the WT plus mutant channels showed a shift to more positive potentials compared with the WT channels (Figure 2F,I,J and Table 3). The $\Delta V_{1/2}$ ($V_{1/2}(\text{p.A172T/}$

WT)- $V_{1/2}(\text{WT})$) values were +22 mV at 0 mM [Mg^{2+}] and +37 mV at 10 mM [Mg^{2+}] ($P < .001$) (Figure 2J and Table 3). The data suggest that Mg^{2+} dependency of channel activation was reduced by the p.(A172T) variant. Co-immunoprecipitation (Co-IP) assays showed that FLAG-tagged WT channels or variant BK channels interacted with GFP-tagged WT BK channels (Figure 2K). These data suggest that WT and mutant BK channel subunits can co-assemble to form heteromeric channels.

Many disease-associated ion channel variants may affect the expression of channel proteins and/or their subcellular distribution on the cell membrane.^{23,24} To explore the impact of genetic variation on the expression of BK channel proteins and BK channel trafficking, we transiently transfected expression plasmids for WT *KCNMA1*-FLAG or variant *KCNMA1*-FLAG into HEK293T cells, and used them for Western blot analysis with an anti-Flag antibody. Both the total protein and membrane protein expression levels of variant *KCNMA1*-FLAG and WT *KCNMA1*-FLAG were essentially equal (Figure 2L-N, Figure S2). The data indicate

FIGURE 2 *KCNMA1* variant p.(A172T) acts by a loss-of-function mechanism. (A) Pedigree structure and genotyping data for *KCNMA1* variant p.(A172T) showing the de novo nature of the variant. (B) The p.(A172T) variant occurs at an evolutionarily conserved amino acid residue. (C-J) Electrophysiological characterization of the p.(A172T) variant. (C and D) Representative macroscopic currents and G-V curves of WT, WT + p.(A172T), or p.(A172T) BK channels from inside-out patch experiments in the presence of 10 μ M Ca^{2+} using the protocol indicated at the left ($n = 17-25/\text{group}$). (E) The p.(A172T) variant reduced the normalized amplitude of BK currents by more than 90% when expressed by itself and by 35%-60% when expressed with WT channels ($^{\ddagger}P < .001$). (F-H) Effects of the p.(A172T) variant on Ca^{2+} -dependent activation of BK currents. (F and G) Representative macroscopic currents and G-V curves of WT and WT + p.(A172T) BK channels recorded using the protocol in F panel at nominal 0 μ M [Ca^{2+}], 1 μ M [Ca^{2+}] and 10 μ M [Ca^{2+}]. All G-V curves were fitted by Boltzmann function (solid lines) with $V_{1/2}$ and slope factors at nominal 0 μ M Ca^{2+} , 1 μ M Ca^{2+} and 10 μ M Ca^{2+} ($n = 17-25/\text{group}$). (H) Relationship between $V_{1/2}$ and [Ca^{2+}]_i from the data in the G panel ($^{\ddagger}P < .001$). (F, I, and J) Effects of the p.(A172T) variant on Mg^{2+} -dependent activation of BK currents. (F and I) Representative macroscopic currents and G-V curves of WT and WT + p.(A172T) channels recorded in 0 and 10 mM [Mg^{2+}] using the protocol in the F panel. All G-V curves were fitted by Boltzmann function (solid lines) ($n = 17-25/\text{group}$). (J) Relationship between $V_{1/2}$ and [Mg^{2+}]_i from the data in the I panel ($^{\ddagger}P < .001$). (K) Co-IP showing interaction between WT and p.(A172T) channels. (L) Western blot analysis showing that the p.(A172T) variant does not change the total protein and membrane protein levels of BK channels. (M and N) Quantitation of protein levels from the data as in the L panel ($n = 4$)

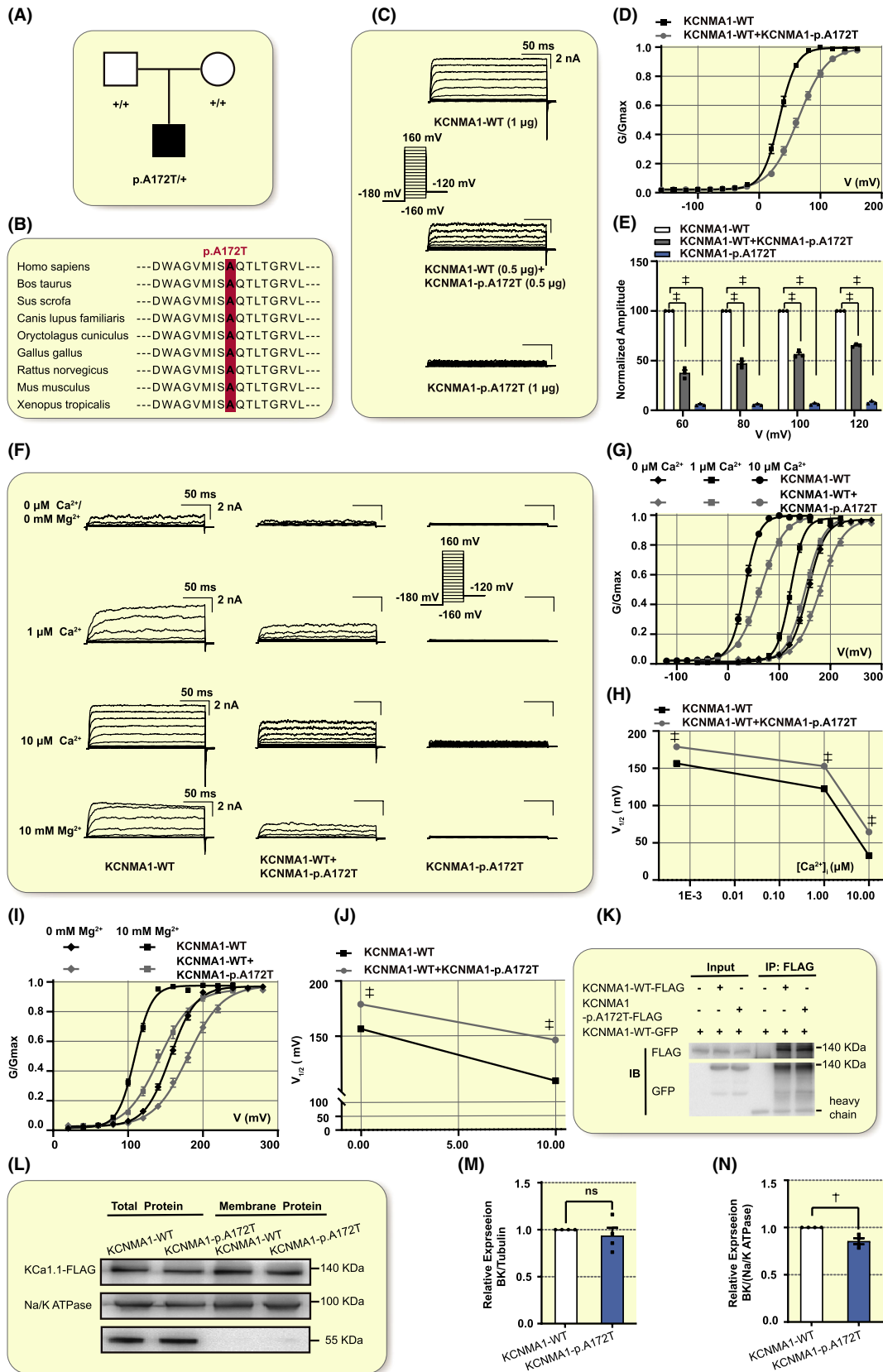


TABLE 2 Summary of diverse clinical features and functional characteristics associated with *KCNMA1* variants

Genomic variant	p.A172T	p.A314T	p.N536H	p.N995S	p.S351Y (13)	p.G354S (34)	p.G356R (13)	p.G375R (13)	p.D434Gly (11)	p.N536H (17)	p.N995S (12)
<i>KCNMA1</i> mutation	c.514G>A	c.940G>A	c.1606A>C	c.2984A>G	c.1052C>A	c.1060G>A	c.1066G>C	c.1123G>A	c.1301A>G	c.1606A>C	c.2984A>G
Location	Helix2 of S0-S1 Loop	S5	RCK1	RCK2	S5-S6	S5-S6	S5-S6	S6	RCK1	RCK1	RCK2
Sex	M	M	F	F	F	M	M/F	M/F	M/F	F	F
DD	Global	Mild to moderate	Moderate	Yes	Mild	Yes	Severe	No	No	No	Yes
ID	NA	Mild	Yes	Moderate	Mild	NA	Yes	Severe	No	Yes	No
Cognitive impairment	Borderline	Mild	Mild	Yes	NA	Mild	Mild	NA	No	NA	No
Ataxia	Yes	Mild	No	NA	Mild	Yes	Yes	No	No	NA	No
Seizures	No	Generalized epilepsy (first seizures at the age of 3 years)	Yes	Yes	No	Febrile	No	Absence	Generalized	Rare epileptiform activity	Myoclonic
Dyskinesia/Dystonia	No	No	Dyskinesia	Dyskinesia	No	Yes	Severe	No	Yes	Yes	No
Dysmorphic features	No	Discrete	Mild	Long face, hypertelorism, bulbous nose, pointed chin	Mild	NA	No	Yes	No	NA	No
BK current properties	No current	Reduced current	Increased current	Increased current	No current	Reduced current	No current	No current	Increased current	NA	Increased current
Total protein	No difference	Reduced protein	Reduced protein	No difference	NA	No difference	NA	NA	NA	NA	NA
Membrane protein	No difference	Reduced protein	Reduced protein	No difference	NA	No difference	NA	NA	NA	NA	NA

Abbreviations: DD, developmental delay; F, female; ID, intellectual disability; M, male; NA, data not available.

TABLE 3 Summary data of BK channel properties under a range of Ca²⁺ and Mg²⁺ concentrations

	0 $\mu\text{M Ca}^{2+}$		1 $\mu\text{M Ca}^{2+}$		10 $\mu\text{M Ca}^{2+}$		0 mM Mg ²⁺		10 mM Mg ²⁺	
	V _{1/2} (mV)	K	V _{1/2} (mV)	K	V _{1/2} (mV)	K	V _{1/2} (mV)	K	V _{1/2} (mV)	K
<i>Group 1 (n = 17-25)</i>										
WT	156.45 ± 2.00	16.41 ± 0.76	122.42 ± 2.09	11.85 ± 0.58	32.77 ± 2.24	12.58 ± 0.23	156.45 ± 2.00	16.41 ± 0.76	108.83 ± 1.24	10.54 ± 0.25
WT + p.A172T	178.75 ± 3.42*	21.74 ± 1.41	152.67 ± 2.93*	17.49 ± 0.76	64.35 ± 3.49*	21.61 ± 0.57	178.75 ± 3.42*	21.74 ± 1.41	145.74 ± 4.06*	19.45 ± 1.24*
p.A172T	-	-	-	-	-	-	-	-	-	-
<i>Group 2 (n = 16-20)</i>										
WT	158.79 ± 2.33	17.64 ± 0.81	118.25 ± 1.76	12.09 ± 0.66	35.77 ± 2.92	14.60 ± 0.41	158.79 ± 2.33	17.64 ± 0.81	106.71 ± 1.60	11.32 ± 0.77
WT + p.A314T	176.00 ± 2.74	21.26 ± 1.23	125.28 ± 1.97	11.68 ± 0.72	47.09 ± 1.25	16.66 ± 0.72	176.00 ± 2.74	21.26 ± 1.23	112.65 ± 2.48	11.40 ± 0.61
p.A314T	184.08 ± 2.75*	22.36 ± 0.93	135.14 ± 1.93*	11.97 ± 0.40	56.51 ± 2.77*	13.39 ± 0.64	184.08 ± 2.75*	22.36 ± 0.93	120.78 ± 1.77*	11.80 ± 0.37*
<i>Group 3 (n = 14-20)</i>										
WT	157.03 ± 2.53	17.16 ± 0.66	121.19 ± 1.95	11.66 ± 0.78	32.95 ± 2.46	12.05 ± 0.42	157.03 ± 2.53	17.16 ± 0.66	106.71 ± 1.60	11.32 ± 0.77
WT + p.N536H	110.71 ± 2.63	18.85 ± 1.07	77.23 ± 3.14	15.07 ± 0.66	13.71 ± 4.28	18.06 ± 1.19	110.71 ± 2.63	18.85 ± 1.07	57.69 ± 2.23	15.07 ± 0.46
p.N536H	66.03 ± 2.31*	13.01 ± 0.90	42.51 ± 1.39*	13.77 ± 0.38	-26.01 ± 2.35*	16.66 ± 0.55	66.03 ± 2.31*	13.01 ± 0.90	18.30 ± 1.42*	8.55 ± 0.55*
<i>Group 3 (n = 14-24)</i>										
WT	158.20 ± 1.84	17.44 ± 0.56	120.96 ± 1.76	12.12 ± 0.63	32.93 ± 2.33	12.61 ± 0.33	158.20 ± 1.84	17.44 ± 0.56	105.99 ± 1.50	11.22 ± 0.70
WT + p.N995S	133.21 ± 1.86	18.40 ± 1.01	82.34 ± 2.47	15.09 ± 1.16	14.37 ± 3.58	15.09 ± 1.16	133.21 ± 1.86	18.40 ± 1.01	82.26 ± 1.67	12.13 ± 0.37
p.N995S	118.26 ± 1.84*	15.80 ± 1.07	44.62 ± 1.47*	18.26 ± 1.32	-14.84 ± 1.61*	18.26 ± 1.32	118.26 ± 1.84*	15.80 ± 1.07	64.61 ± 0.83	10.20 ± 0.32

Note: V_{1/2}, voltage at half-maximal activation; k, slope factor of voltage dependence of activation. Data are presented as mean ± SEM.

*P < .001 versus WT (Student's t test). The experiment was repeated at least three times.

that the p.(A172T) variant does not affect total BK protein expression or its membrane localization.

2.3 | A de novo variant p.(A314T) in the S5 transmembrane segment significantly decreases the protein expression and BK potassium current

A heterozygous de novo variant in the *KCNMA1* gene c.940G>A [p.(A314T)] was identified in a 17-year-old male patient with mild to moderate developmental delay, mild intellectual disability, mild cognitive impairment, mild ataxia and generalized epilepsy (Figures 1 and 3A and Table 2). The patient experienced the first seizure at 3 years of age (Table 2). Alanine 314 is located in the S5 transmembrane segment (Figure 1) and is conserved among BK channels from *Xenopus* to humans (Figure 3B). In silico bioinformatic analysis suggested that the p.(A314T) variant might be deleterious (Mutation Taster; PolyPhen-2; SIFT). Patch-clamp analysis showed that the mean macroscopic amplitude of the BK current generated from cells overexpressing mutant *KCNMA1* with the p.(A314T) missense variant was markedly less than the cells overexpressing WT *KCNMA1* (reduction of 60% at 100 mV, $P < .001$) (Figure 3C,E). Furthermore, the p.(A314T) missense variant led to a shift of the G-V curve towards a more positive potential at 10 μM [Ca^{2+}] by +21 mV ($P < .001$) (Figure 3D and Table 3).

To mimic the heterozygous state of the variant in the patient, we transiently transfected an equal amount of WT and variant plasmids (0.5 μg /plasmid), WT plasmid alone (1 μg) or variant plasmid alone (1 μg) into HEK293T cells and recorded potassium currents. Compared with WT BK channels, WT/mutant heteromeric channels showed

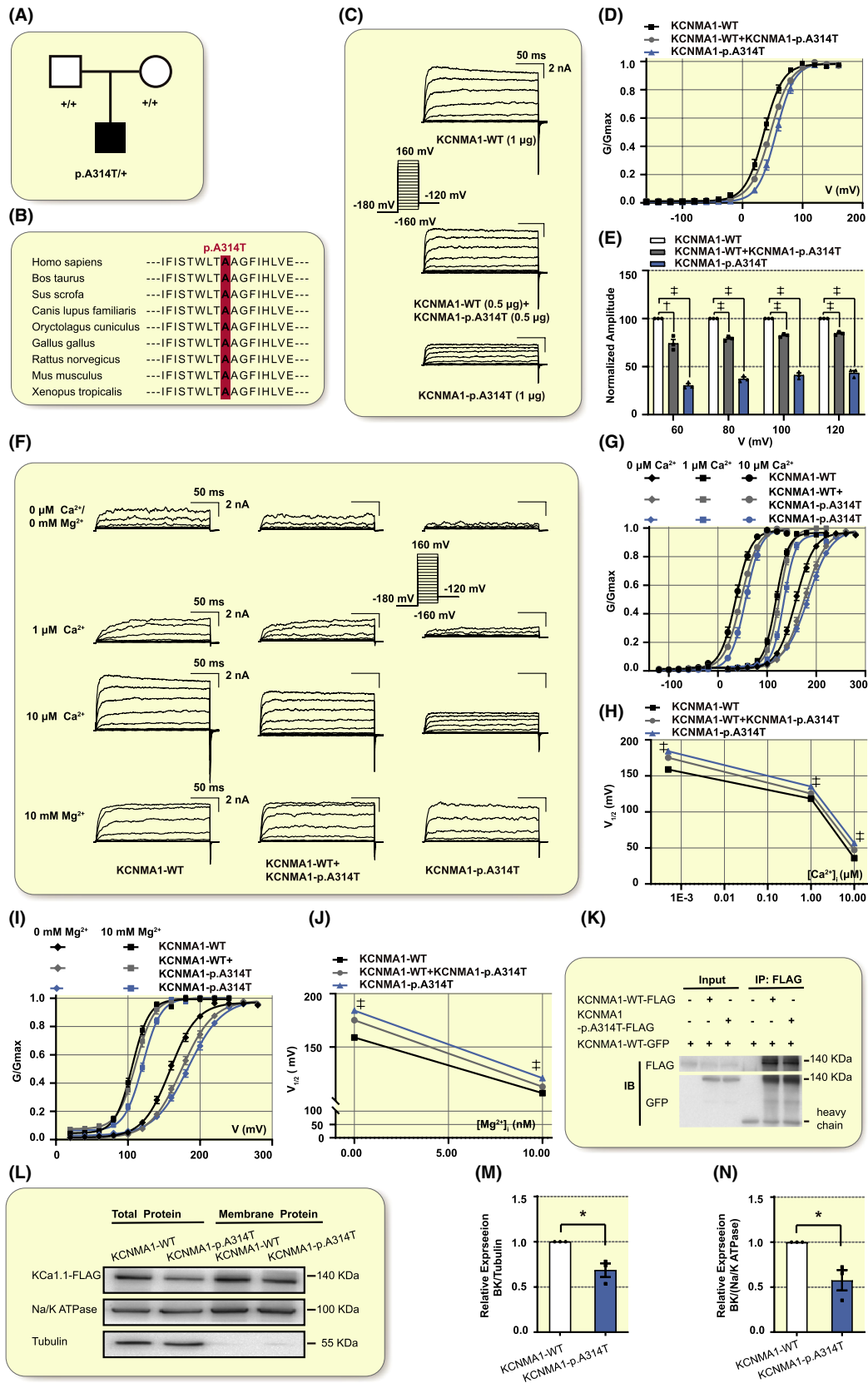
about 16% reduction of the normalized current densities at 100 mV ($P < .001$) (Figure 3C,E), and a more positive voltage at which the channel was half-activated by +12 mV ($P < .001$) (Figure 3D and Table 3). Compared with WT channels, the p.(A314T) variant channels shifted the G-V curves towards more positive potentials about +20 mV at nominal Ca^{2+} concentrations of 0, 1 and 10 μM ($P < .001$) (Figure 3F-H and Table 3). Meanwhile, we examined BK current activation from WT and p.(A314T) variant channels at 0 and 10 mM [Mg^{2+}]. Compared with WT channels, the G-V curves of p.(A314T) variant channels exhibited a shift to more positive potentials by +26 mV in the absence of Mg^{2+} and by +14 mV at 10 mM [Mg^{2+}] (Figure 3I). The $\Delta V_{1/2}$ values were similar at a range of Ca^{2+} and Mg^{2+} concentrations (Figure 3F-J, Table 3). The data indicate that the p.(A314T) variant does not affect $\text{Ca}^{2+}/\text{Mg}^{2+}$ -dependent activation of BK channels.

Co-IP assays showed that there was an interaction between p.(A314T) variant channels and WT channels (Figure 3K). Furthermore, Western blot analysis showed that both the total protein and membrane protein expression levels of the p.(A314T) variant channels were decreased by approximately 35% compared with WT channels ($P < .05$) (Figure 3L-N, and Figure S3). The data further indicate that p.(A314T) is a LOF variant.

2.4 | A de novo variant p.(N536H) in the RCK1 domain of BK channels is associated with intellectual disability, developmental delay, epilepsy, paroxysmal dyskinesia, mild cognitive impairment and mild dysmorphic features

A de novo *KCNMA1* variant, c.1606A>C [p.(N536H)], was identified in a female patient with intellectual disability,

FIGURE 3 3 *KCNMA1* variant p.(A314T) acts by a loss-of-function mechanism. (A) Pedigree structure and genotyping data for *KCNMA1* variant p.(A314T) showing the de novo occurrence of the p.(A314T) variant. (B) The p.(A314T) variant occurs at an evolutionarily conserved amino acid residue. (C-J) Electrophysiological characterization of the p.(A314T) variant. (C and D) Representative macroscopic currents and G-V curves of WT, WT + p.(A314T), or p.(A314T) BK channels from inside-out patch experiments in the presence of 10 μM [Ca^{2+}] using the protocol indicated at the left ($n = 16-20/\text{group}$). (E) The p.(A314T) variant reduced the normalized amplitude of BK current by 60%-70% when expressed alone and by about 25% when co-expressed with WT channels ($^{\ddagger}P < .001$, $^{\dagger}P < .01$). (F-H) Effects of the p.(A314T) variant on Ca^{2+} -dependent activation of BK currents. (F and G) Representative macroscopic currents and G-V curves of WT, WT + p.(A314T) and p.(A314T) BK channels recorded using the protocol in F at nominal 0 μM [Ca^{2+}], 1 μM [Ca^{2+}] and 10 μM [Ca^{2+}]. All G-V curves were fitted by Boltzmann function (solid lines) with $V_{1/2}$ and slope factors at nominal 0 μM [Ca^{2+}], 1 μM [Ca^{2+}] and 10 μM [Ca^{2+}] ($n = 16-20/\text{group}$). (H) Relationship between $V_{1/2}$ and [Ca^{2+}]_i from the data as in the G panel ($^{\ddagger}P < .001$). (F, I, and J) Effects of the p.(A314T) variant on Mg^{2+} -dependent activation of BK currents. (F and I) Representative macroscopic currents and G-V curves of WT, WT + p.(A314T) and p.(A314T) channels recorded at 0 and 10 mM [Mg^{2+}] using the protocol in the F panel. All G-V curves were fitted by Boltzmann function (solid lines) ($n = 16-20/\text{group}$). (J) Relationship between $V_{1/2}$ and [Mg^{2+}]_i from the data in the I panel ($^{\ddagger}P < .001$). (K) Co-IP assays showing interaction between WT and p.(A314T) channels. (L) Western blot analysis showing that the p.(A314T) variant reduced the total protein and membrane protein levels of BK channels. (M and N) Quantitation of protein levels from the data as in the L panel ($n = 3$; $^{\ast}P < .05$)



developmental delay, epilepsy, paroxysmal dyskinesia, mild cognitive impairment and mild dysmorphic features (Figures 1 and 4A and Table 2). Asparagine 536 is located in

the Ca^{2+} -sensing RCK1 domain that contains a high-affinity Ca^{2+} -binding site (Figure 1)^{25,26} and is highly conserved through evolution (Figure 4B). Compared with WT channels,

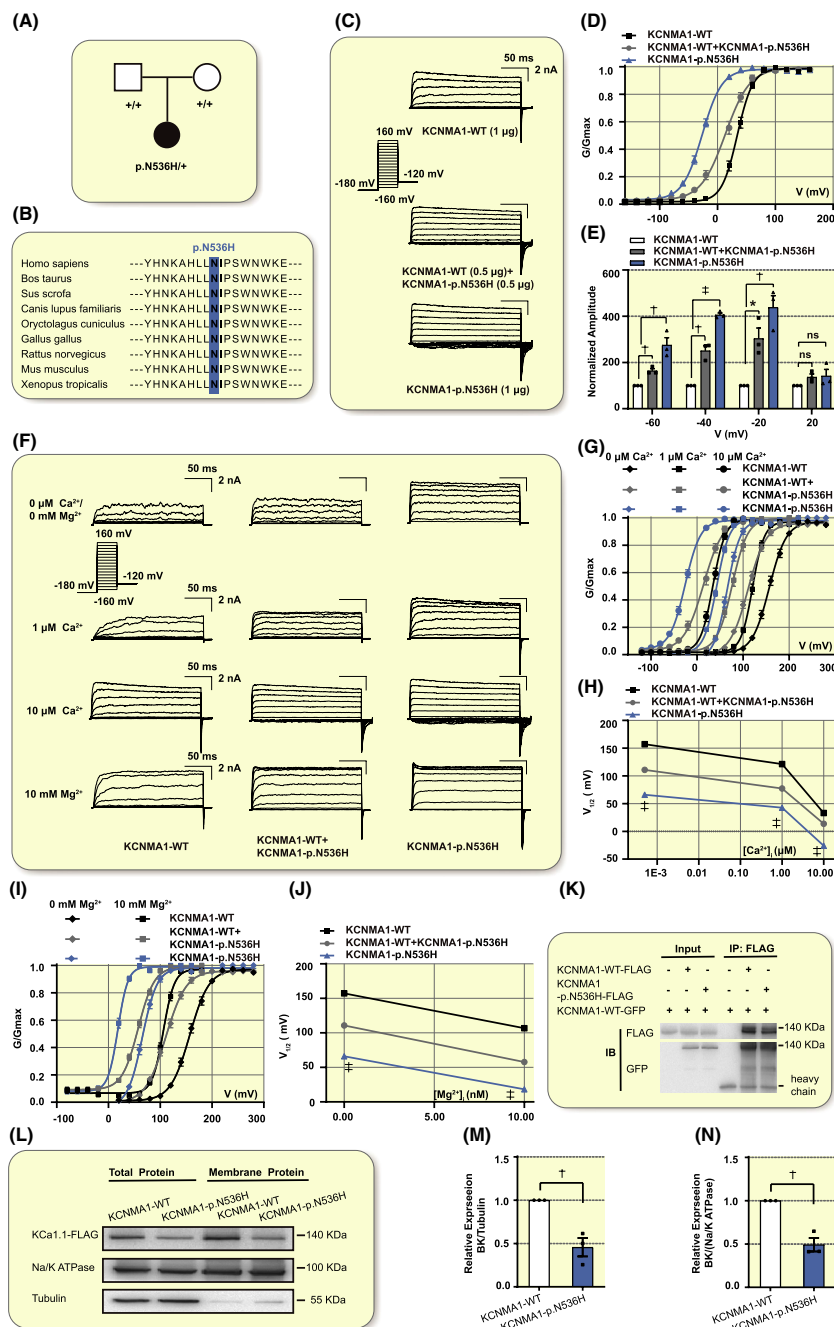


FIGURE 4 *KCNMA1* variant p.(N536H) acts as a gain-of-function mechanism. (A) Pedigree structure and genotyping data for *KCNMA1* variant p.(N536H) showing the de novo occurrence of the variant. (B) The p.(N536H) variant occurs at an evolutionarily conserved amino acid residue. (C-J) Electrophysiological characterization of the p.(N536H) variant. (C and D) Representative macroscopic currents and G-V curves of WT, WT + p.(N536H), and p.(N536H) BK channels from inside-out patch experiments in the presence of 10 μM $[\text{Ca}^{2+}]_i$ using the protocol indicated at the left ($n = 14-20/\text{group}$). (E) The p.(N536H) variant increased the normalized amplitude of BK currents by more than 300% when expressed alone and by 200% when co-expressed with WT channels at -20 mV ($^{\ddagger}P < .001$, $^{\dagger}P < .01$, $^*P < .05$). (F-H) Effects of the p.(N536H) variant on Ca^{2+} -dependent activation of BK currents. (F and G) Representative macroscopic currents and G-V curves of WT, WT + p.(N536H) and p.(N536H) BK channels at nominal 0 μM $[\text{Ca}^{2+}]_i$, 1 μM $[\text{Ca}^{2+}]_i$ and 10 μM $[\text{Ca}^{2+}]_i$. G-V curves were fitted by Boltzmann function (solid lines) with $V_{1/2}$ and slope factors at nominal 0 μM $[\text{Ca}^{2+}]_i$, 1 μM $[\text{Ca}^{2+}]_i$ and 10 μM $[\text{Ca}^{2+}]_i$ ($n = 14-20/\text{group}$). (H) Relationship between $V_{1/2}$ and $[\text{Ca}^{2+}]_i$ from the data in the G panel ($^{\ddagger}P < .001$). (F, I, and J) Effects of the p.(N536H) variant on Mg^{2+} -dependent activation of BK currents. (F and I) Representative macroscopic currents and G-V curves recorded at 0 and 10 mM $[\text{Mg}^{2+}]_i$ for WT, p.(N536H) and WT + p.(N536H) channels using the protocol in the F panel. All the G-V curves were fitted by Boltzmann function (solid lines) ($n = 14-20/\text{group}$). (J) Relationship between $V_{1/2}$ and $[\text{Mg}^{2+}]_i$ from the data as in the I panel ($^{\ddagger}P < .001$). (K) Co-IP assays showing interaction between WT and p.(N536H) channels. (L) Western blot analysis showing that the p.(N536H) variant reduced the total protein and membrane protein levels of BK channels. (M and N) Quantitation of protein levels from the data as in the L panel ($n = 3$; $^{\dagger}P < .01$)

the variant p.(N536H) channels significantly increased the mean amplitude of the BK current and shifted the G-V curves to more negative potentials by -58 mV at $10 \mu\text{M}$ $[\text{Ca}^{2+}]$ ($P < .001$, Figure 4C-E and Table 3). The mean current amplitude and the extent of negative shift of the G-V curve for the hetero-WT/mutant channels were about half of the mutant channels compared with WT channels (Figure 4C-E). This data suggest that p.(N536H) is a GOF variant.

We also investigated the impact of the p.(N536H) variant on Ca^{2+} - and Mg^{2+} -dependent activation of BK currents. The G-V curves of the p.(N536H) channels shifted to more negative potentials compared with those of WT channels at all Ca^{2+} concentrations. The shift was approximately -80 mV in the presence of $1 \mu\text{M}$ intracellular $[\text{Ca}^{2+}]$ and approximately -100 mV in the presence of $0 \mu\text{M}$ intracellular $[\text{Ca}^{2+}]$, suggesting a small degree of reduced sensitivity of the mutant or hetero-WT/mutant channels to Ca^{2+} -dependent activation ($P < .001$) (Figure 4F-H and Table 3). In contrast, the variant did not affect the sensitivity to Mg^{2+} (Figure 4F,I,J and Table 3).

Co-IP assays showed that the FLAG-tagged WT or mutant BK channels interacted with GFP-tagged WT BK channels (Figure 4K). In addition, we transfected cells with expression plasmids for the WT or variant p.(N536H) *KCNMA1* and analysed their expression levels by Western blotting. The total protein and membrane protein levels of the p.(N536H) variant channels were decreased by approximately 55% compared with WT channels ($P < .01$) (Figure 4L-N, and Figure S4).

2.5 | A de novo variant p.(N995S) is associated with developmental delay, cognitive impairment, moderate intellectual disability, epilepsy, dyskinesia and dysmorphism

We identified a 17-year-old female patient who had developmental delay, cognitive impairment, moderate intellectual disability, partial epilepsy and dyskinesia (Figure 5A and Table 2). She also showed microcephaly and some dysmorphic features including long face, hypertelorism, bulbous nose and pointed chin. Interictal electroencephalography (EEG) revealed multifocal bilateral epileptiform discharges (Table 2). Brain magnetic resonance imaging and metabolic analysis results were normal. Mutational analysis identified a de novo missense *KCNMA1* variant [c.2984A>G, p.(N995S)] from the patient (Figures 1 and 5A and Table 2). Asparagine 995 is located in the RCK1 domain and conserved from *Xenopus* to humans (Figure 5). Interestingly, we previously reported the same variant in two independent patients who had epilepsy in early childhood, but without

paroxysmal dyskinesia.¹² Here, electrophysiological studies indicated that the p.(N995S) variant significantly enhanced the BK potassium currents and shifted the voltage at which the current was half-activated towards more negative potentials compared with that of the WT channels by -46 mV at $10 \mu\text{M}$ $[\text{Ca}^{2+}]$ ($P < .001$) (Figure 5D and Table 3). Our previous study showed that the p.(N995S) variant promoted voltage-dependent activation of BK channels and shortened the channel activation time.¹² In this study, we also characterized the function of mutant BK channels in a heterozygous state. Compared with WT channels, the shift of the G-V curve to more negative potentials by hetero-WT/mutant channels were about 50% of that for mutant channels (Figure 5D). In contrast, compared with WT channels, the enhancement of the normalized current amplitude for hetero-WT/mutant channels were much less than that for mutant channels at negative potentials (Figure 5D). The data may suggest that the effect of the p.(N995S) variant on BK channels was somehow reduced in the heterozygous state compared with the homozygous mutant state. As reported previously, the p.(N995S) variant had a minimal effect on the Ca^{2+} -dependent activation of BK channels (Figure 5F-H). Similarly, the p.(N995S) variant had no effect on the Mg^{2+} -dependent activation of BK channels (Figure 5F,I,J). Co-IP assays showed that the mutant channels interacted with WT channels to co-assemble heteromeric channels (Figure 5K). Western blot analysis showed that variant p.(N995S) neither affected the expression level of total protein nor that of the membrane BK channel proteins (Figure 5L-N, and Figure S5).

3 | DISCUSSION

Liang-Wang syndrome (MIM #618729) is a newly reported polymalformation disease with a wide spectrum of developmental and neurological abnormalities, and caused by LOF pathogenic variants in BK channel gene *KCNMA1*.¹³ Because Liang-Wang syndrome is a new syndrome and presented a large variability on clinical manifestation,¹³ the correlation between clinical phenotypes and genotypes needs further extensive investigation. In this study, we described the detailed functional and biophysical characteristics of four variants in the BK channel. We found two new *KCNMA1* variants, p.(A172T) and p.(A314T), that act by a LOF mechanism and cause Liang-Wang syndrome. The patient with p.(A172T) had global developmental delay, borderline cognitive impairment and ataxia but without paroxysmal dyskinesia, seizures or dysmorphic features. The patient with p.(A314T)

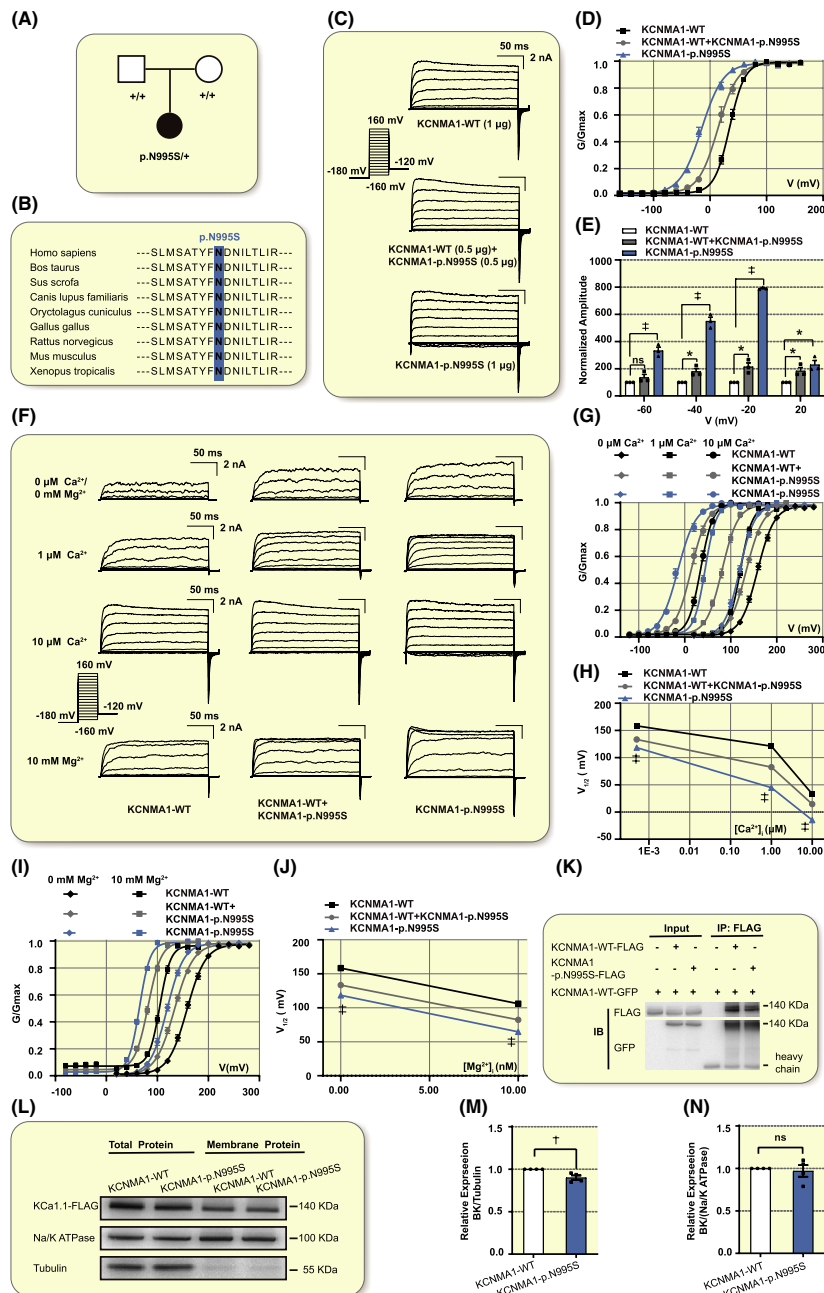


FIGURE 5 *KCNMA1* variant p.(N995S) acts by a gain-of-function mechanism. (A) Pedigree structure and genotyping data for *KCNMA1* variant p.(N995S) showing the de novo occurrence of the variant. (B) The p.(N995S) variant occurs at an evolutionarily conserved amino acid residue. (C-J) Electrophysiological characterization of the p.(N995S) variant. (C and D) Representative macroscopic currents and G-V curves of WT, WT + p.(N995S), and p.(N995S) BK channels from inside-out patch experiments in the presence of 10 μM $[\text{Ca}^{2+}]_i$ using the protocol indicated at the left ($n = 14-24/\text{group}$). (E) The p.(N995S) variant increased BK current by more than 600% when expressed alone and by 100% when co-expressed with WT channels ($^{\ddagger}P < .001$, $^*P < .05$). (F-H) Effects of the p.(N995S) variant on Ca^{2+} -dependent activation of BK currents. (F and G) Representative macroscopic currents and G-V curves of WT, WT + p.(N995S), and BK channels recorded at nominal 0 μM $[\text{Ca}^{2+}]_i$, 1 μM $[\text{Ca}^{2+}]_i$ and 10 μM $[\text{Ca}^{2+}]_i$. G-V curves were fitted by Boltzmann function (solid lines) with $V_{1/2}$ and slope factors at nominal 0 μM $[\text{Ca}^{2+}]_i$, 1 μM $[\text{Ca}^{2+}]_i$ and 10 μM $[\text{Ca}^{2+}]_i$ ($n = 14-24/\text{group}$). (H) Relationship between $V_{1/2}$ and $[\text{Ca}^{2+}]_i$ from the data in the G panel ($^{\ddagger}P < .001$). (F, I, and J) Effects of the p.(N995S) variant on Mg^{2+} -dependent activation of BK currents. (F and I) Representative macroscopic currents and G-V curves for BK currents recorded at 0 and 10 mM $[\text{Mg}^{2+}]_i$ for WT, p.(N995S), and WT + p.(N995S) channels using the protocol in F panel. All the G-V curves were fitted by Boltzmann function (solid lines) ($n = 14-24/\text{group}$). (J) Relationship between $V_{1/2}$ and $[\text{Mg}^{2+}]_i$ from the data in the I panel ($^{\ddagger}P < .001$). (K) Co-IP assays showing interaction between WT and p.(N995S) channels. (L) Western blot analysis showing that the p.(N995S) variant does not change the total protein and membrane protein levels of BK channels. (M and N) Quantitation of protein levels from the data as in the L panel ($n = 4$)

had mild to moderate developmental delay, mild intellectual disability, mild cognitive impairment, mild ataxia and generalized epilepsy. These data significantly expand the spectrum of *KCNMA1* LOF variants associated with Liang–Wang syndrome.

We also identified two new patients with previously reported GOF *KCNMA1* variants, p.(N536H) and p.(N995S), and characterized them both clinically and functionally in more details. We reported that GOF variants of *KCNMA1*, p.(D434G) and p.(N995S), were associated with generalized epilepsy, paroxysmal dyskinesia or both (GEPD).^{11,12} Surprisingly, our new patient with the p.(N536H) GOF variant showed much more complex phenotypes, including intellectual disability, developmental delay, mild cognitive impairment, epilepsy, mild dysmorphic features and paroxysmal dyskinesia (Table 2). Zhang et al described the same p.(N536H) variant from an unrelated patient in 2020.¹⁸ Compared with our patient with a clear diagnosis of epilepsy, the patient reported by Zhang and colleagues had rare epileptiform activity without any EEG correlate.¹⁸ In addition, our patient displayed developmental delay, mild cognitive impairment and mild dysmorphic features, while the patient from Zhang et al displayed symptoms of autism spectrum disorder, mild cerebellar atrophy and an attention deficit hyperactivity disorder.¹⁸ Similarly, our new patient with the p.(N995S) GOF variant showed much more complex phenotypes, including developmental delay, cognitive impairment, moderate intellectual disability, partial epilepsy, dyskinesia, microcephaly, some dysmorphic features including long face, hypertelorism, bulbous nose, and pointed chin, multifocal bilateral epileptiform discharges on EEGs, and normal brain MRI and metabolic analysis (Table 2). These new data significantly expand the spectrum of clinical features associated with GOF variants of *KCNMA1*.

Notably, with more and more genotype–phenotype correlation studies reported, clinical features associated with GOF variants (GEPD) and LOF variants (Liang–Wang syndrome) of *KCNMA1* appear to overlap in a large extent, although distinct differences were also noted. To date, there are three GOF *KCNMA1* variants that have been reported and functionally characterized in details, including p.(D434G) identified in a large family, p.(N995S) identified in seven independent patients and p.(N536S) identified in a single patient (Figure 6).^{11,12,17,18} A total of nine LOF variants were reported and functionally characterized, including p.(S351Y), p.(G354R), p.(G356R), p.(G375R), p.(C413Y)/p.(N449fs), p.(I663V), p.(P805L) and p.(D984N)^{13,27} (Figure 6). Two reported mutations, p.(R458X) and p.(Y676Lfs*7),^{15–17} were assumed to act by a LOF mechanism because of the stop codon change and frame-shift. However, we found a non-peer reviewed

report in ‘Research Square’ stating that p.(R458X) acted by a GOF mechanism because the mutation increased potassium current in Michigan Cancer Foundation 7 (MCF 7) cells.²⁸ As shown in Figure 6A, GOF *KCNMA1* variants and LOF variants share some clinical features, including epilepsy, developmental delay, intellectual disability and movement disorders. However, differences are also clear for the two types of mutations. First, LOF variants cause visceral malformations and facial dysmorphism (Figure 6A). Second, the type of movement disorders is different: GOF *KCNMA1* variants cause paroxysmal non-kinesigenic dyskinesia, but LOF variants cause ataxia and tremor (Figure 6A). Similarly, the clinical features for the two GOF *KCNMA1* variants (p.(N536H) and p.(N995S)) and two LOF variants p.(A172T) and p.(A314T) described in this study show similarities and differences (Figure 6B). In addition to shared features of epilepsy, developmental delay, intellectual disability and movement disorders, both types of variants also share cognitive impairment, microcephaly and some dysmorphic features (long face, hypertelorism, bulbous nose, pointed chin) (Figure 6B). On the other hand, for movement disorders, GOF *KCNMA1* variants cause paroxysmal dyskinesia, but LOF variants cause ataxia (Figure 6B).

The p.(A172T) variant identified in a Liang–Wang syndrome patient occurs in the intracellular loop between S0 and S1. We found that mutant BK channels with p.(A172T) failed to elicit any potassium current (Figure 2C,D), although it did not affect the expression level of either total or membrane-bound BK channels (Figure 2L–N). Our data are consistent with the characteristics of the S0–S1 loop reported from previous studies showing that the S0–S1 loop plays a substantial role in regulating the BK channel function.²⁹ The physical interaction between the auxiliary subunit(s) and S0 segment of the BK channel α -subunit is crucial for fine-tuning the properties of BK channels in different tissues.³⁰ Jeffries et al showed that palmitoylation within the S0–S1 linker region could regulate the plasma membrane expression of BK channel.³¹ Further, Duncan et al revealed that the S0–S1 loop contained a specific post-translational modification site for S-acylation, whereas the S-acylation of the α -subunits of BK can dynamically regulate the functional coupling between the α -subunits of the BK channel and the β 1-subunits.³² Further secondary structure analysis predicted special Helix1 and Helix2 within the S0–S1 loop.³³ The affected Ala172 is located in a fairly critical Helix2 site (Trp158 to Leu175).³⁴ Suzuki et al revealed that the deletion mutant of Δ 171–178 affected both the macroscopic BK currents and the cell surface expression of the BK channel.³⁴ However, substitution of Ser¹⁷¹ or Gln¹⁷³ to an alanine residue significantly decreased the potassium currents due to a shift of G–V

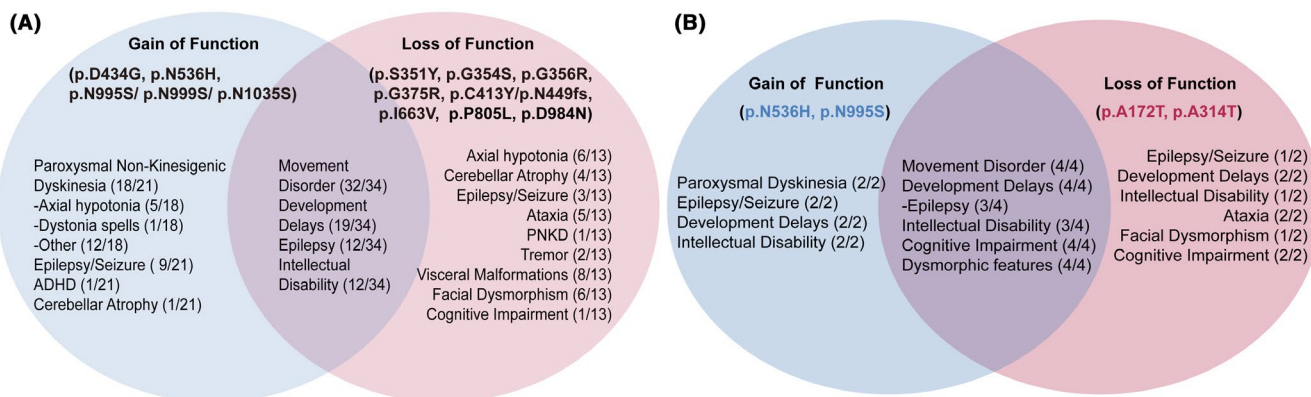


FIGURE 6 Genotype–phenotype correlation studies identify clinical features of Liang–Wang syndrome caused by loss-of-function variants of *KCNMA1*, clinical features associated with by gain-of-function variants of *KCNMA1*, and clinical features shared by both loss-of-function and gain-of-function variants of *KCNMA1*. (A) Genotype-phenotype correlation studies for previously reported *KCNMA1* variants. (B) Genotype-phenotype correlation studies for the four variants characterized in this study

curves to more positive potentials, but had no influence on cell surface expression of the BK channel.³⁴ Asp¹⁶⁴ was reported to provide an Mg²⁺-binding site, and Mg²⁺ can mediate the interaction between the voltage-sensor domain and the cytoplasmic domain. Substitution of the Mg²⁺-binding residue, Asp164, with alanine abolishes Mg²⁺ sensitivity.²² Recently, Laumonier et al found that a *KCNMA1* SNP p.(A138V) located in the S0-S1 loop was associated with autism and led to reduced BK current in the lymphoblastoid cell lines of patients.³⁵ Interestingly, Plante et al showed that this SNP altered the sensitivity of the BK channel to Mg²⁺-dependent gating under 1 μ M Ca²⁺ condition.³⁶ Our study identified a LOF variant, p.(A172T), that affects a new key amino acid residue that regulates Mg²⁺-dependent gating of BK channels and plays a critical role in the pathogenesis of Liang–Wang syndrome.

It is interesting to note that almost all *KCNMA1* variants, either GOF or LOF variants identified to date, are heterozygous de novo variants, which are expected to show an autosomal dominant inheritance pattern in future generations. Two exceptional cases are noted. In one large family with multiple patients affected with epilepsy, paroxysmal dyskinesia, or both, we identified heterozygous *KCNMA1* variant p.(D434G) that shows an autosomal dominant inheritance pattern in the family.¹¹ In one other family, the proband with clinical features of Liang–Wang syndrome carries compound heterozygous *KCNMA1* variants, including the maternally inherited missense variant p.(C413Y) and the frameshift variant p.(N449fs), which is inherited from the father. Functional studies showed that the both variants are LOF variants.¹³ It is also interesting to note that two new *KCNMA1* variants were reported while this manuscript was under consideration. Graber

et al reported a de novo heterozygous one bp deletion variant in *KCNMA1* (c.112delG) in a Liang–Wang syndrome patient who presented with drug-resistant epilepsy with severe developmental delay initially related to bilateral asymmetric frontal polymicrogyria since the age of 2 months.³⁷ Yao et al reported another de novo LOF *KCNMA1* variant, p.(E155Q), in a Liang–Wang syndrome patient with febrile seizures, hyperactivity, repeated daze, poor language development and developmental delay.³⁸

In summary, in this study, we characterized four new patients with *KCNMA1* variants, including p.(A172T), p.(A314T), p.(N536H) and p.(N995S), in detail. We found that two of these variants, p.(A172T) and p.(A314T), acted by a LOF mechanism, and were associated with Liang–Wang syndrome. For two other variants, p.(N536H) and p.(N995S), that acted by a GOF mechanism, new clinical phenotypes were identified, including developmental delay, cognitive impairment, intellectual disability, microcephaly and dysmorphic features. The data expanded the spectrum of *KCNMA1* variants, and the spectrum of clinical features associated with *KCNMA1* variants, and emphasized the interesting finding that LOF and GOF variants of *KCNMA1* shared more clinical features than previously thought. However, much more genotype–phenotype correlation studies are needed in the future to continue to enrich the spectrum of clinical features of Liang–Wang syndrome.

4 | MATERIALS AND METHODS

All the materials submitted conform with good publishing practice in physiology according to Acta Physiologica guidelines.³⁹

4.1 | Patients and *KCNMA1* variants

Patients carrying *KCNMA1* variants were referred to our laboratory for consultation of the functionality by genetic counselors, medical/clinical geneticists or physicians. These patients had whole-exome sequencing performed by certified commercial companies, and sought genetic consultation from their genetic counselors, medical geneticists or physicians, who in turn communicated with us. Exome sequencing was performed using genomic DNA isolated with standard methods from whole blood from proband and parents. Libraries were prepared using the Ion AmpliSeq™ Exome Kit (Life Technologies) and quantified by qPCR. The enriched libraries were prepared using Ion Chef™ and sequenced on PI™ Chip in the Ion Proton™ System (Life Technologies) to provide >90% of amplicons covered with at least 20X. Signal processing, base calling, alignment and variant calling were performed on a Proton™ Torrent Server using the Torrent Suite™ Software. Variants were annotated using Ion Reporter™ Software, and pedigree analysis was performed using the Genetic Disease Screen (GDS) trio workflow. Variant filtering and prioritization and evaluation of list of candidate variants were performed as previously described.⁴⁰ Information from specific databases including variants already described in association with a known phenotype (ClinVar) and population frequency databases (dbSNP, gnomAD, 1000 Genome Project, or NHLBI-ESP 6500 exomes) to annotate variants that usually exist in the general population was used. We also estimated the pathogenicity of variants using CADD and a summation of selected prediction systems included in the dbNSFP database (SIFT, PolyPhen2, MutationTaster, MutationAssessor, LRT, FATHMM, and MetaSVM) for missense mutations. For mutations identified in splicing regions (including synonymous mutations), the effect on mRNA processing has been evaluated using the SpliceSiteFinder and MaxEntScan prediction systems, included in the SPiCE algorithm. Nucleotide position conservation has been evaluated according to the UCSC score ranges for the PhyloP tool. Finally, prioritization variant was based on stringent assessments at both the gene and variant levels, and taking into consideration patient's phenotype and the associated inheritance pattern. Candidate variants were visualized using IGV (Integrative Genomics Viewer). Candidate variants were evaluated based on stringent assessments at both the gene and variant levels, taking into consideration both the patient's phenotype and the inheritance pattern. Variants were classified following the guidelines of the American College of Medical Genetics and Genomics (ACMG).²¹ A board of molecular clinical geneticist

evaluated each variant classified as pathogenic, likely pathogenic, or a variant of uncertain significance, and decided which, if any, had to be reported. In every case, causal variants were discussed with the referring physician and/or clinical geneticist. Identified variants were confirmed by Sanger sequencing. No pathogenic or likely pathogenic variants were identified in genes previously reported for epilepsy, paroxysmal dyskinesia and other movement disorders, and neurodevelopmental disorders. This study was approved by the Ethics Committee of Huazhong University of Science and Technology and other local IRBs on human subject research. Written informed consent was obtained from study subjects according to the appropriate IRB policies. The study abides by the Declaration of Helsinki principles.

4.2 | Plasmids and mutagenesis

An expression plasmid for FLAG-tagged *KCNMA1* (*KCNMA1*-FLAG) (GenBank accession number U23767) was described previously.^{12,13} *KCNMA1* expression plasmids with different variants were constructed using polymerase chain reaction (PCR)-based site-directed mutagenesis.⁴¹ The *KCNMA1* cDNA was also subcloned into the pEGFP-N1 vector to generate an expression plasmid for EGFP-tagged *KCNMA1* (*KCNMA1*-GFP). Primers for molecular cloning are given in Table S1. The entire *KCNMA1* cDNA insert in various plasmids was confirmed by Sanger sequencing as described in our previous study.⁴²

4.3 | Cell culture, transfection and antibodies

HEK293T cells were cultured at 37°C in an incubator with 5% CO₂ in DMEM (Dulbecco's Modified Eagle's Medium) supplemented with 10% fetal bovine serum (FBS) (Gibco, Gaithersburg, MD, USA). For the patch-clamping study, HEK293T cells were cultured to 80% confluence on coverslips in 24-well plates, and transiently transfected with 1 µg of WT *KCNMA1*-FLAG, 0.5 µg of WT *KCNMA1*-FLAG plus 0.5 µg of mutant *KCNMA1*-FLAG, or 1 µg of mutant *KCNMA1*-FLAG together with 0.1 µg of pEGFP-N1 as a transfection indicator using GenJet (SignaGen Laboratories, Rockville, MD, USA). Only cells with green signals were selected for patch-clamping recordings of potassium currents.

The mouse monoclonal anti-FLAG antibody (MBL International, Woburn, MA, USA) and an anti-GFP antibody (Affinity Biosciences, USA) were used at a dilution factor of 1:1000. A mouse anti-β-tubulin antibody

(Millipore, Burlington, MA, USA) and a rabbit anti-Na/K-ATPase antibody (Proteintech, Rosemont, IL, USA) were each used at a dilution factor of 1:1000. A goat anti-mouse horseradish peroxidase (HRP)-conjugated secondary antibody and a goat anti-rabbit HRP conjugated secondary antibody were purchased from Biosharp (China) and each used at a dilution factor of 1:20,000.

4.4 | Co-immunoprecipitation (Co-IP) assays and Western blot analysis

Co-IP assays were performed as previously described.^{43,44} Three groups of plasmids, including p3 x FLAG (8 µg) plus KCNMA1-GFP (8 µg), KCNMA1-FLAG (8 µg) plus KCNMA1-GFP (8 µg), and KCNMA1-mutant-FLAG (8 µg) plus KCNMA1-GFP (8 µg), were respectively transfected into HEK293T cells in 10 cm plates using GenJet (SignaGen Laboratories, Rockville, MD, USA) and cultured for 48 h. The cells then were lysed in ice-cold IP lysis buffer (20 mM Tris-HCl, 150 mM NaCl, 1% Triton-X-100, pH = 7.5), incubated with 1.5 mg of an anti-FLAG antibody at 4°C for 12 h, and mixed with Protein A/G beads (Santa Cruz Biotechnology, USA). Then, the beads were washed 10 times for 2 h using the IP lysis buffer, mixed with 1× SDS-PAGE loading buffer, and analysed by Western blot analysis as described.⁴³

4.5 | Membrane protein isolation

Membrane proteins were prepared by ultracentrifugation and sonication of transfected cells. After 48 h, HEK293T cells were transiently transfected with 5 µg of either the WT plasmid or variant *KCNMA1* expression plasmid in 6 cm plates using 10 µL Lipofectamine 2000 (Invitrogen, Carlsbad, CA, USA). The cells were resuspended in Buffer 1 (25 mM Tris-HCl, 5 mM ethylenediaminetetraacetic acid and 5 mM Ethylenebis tetraacetic acid (EGTA), pH 7.5). One-tenth of the lysates were reserved for total protein analysis while the remaining lysates were subjected to sonication and ultracentrifugation for preparation of membrane proteins. Then, the pellet was washed three times with phosphate-buffered saline (PBS), resuspended in Buffer 2 (20 mM Tris-HCl, 137 mM NaCl, 10% glycerol and 1% Nonidet P-40, pH 7.4), and analysed by Western blotting analysis with an anti-Flag antibody (MBL International, USA) as described previously.⁴⁵

4.6 | Electrophysiological analysis

For patch-clamping experiments, the BK potassium current was recorded using an inside-out configuration

with an Axon MultiClamp 700B patch clamp amplifier and a Digidata 1440A converter (Axon Instruments, San Jose, CA, USA) with pCLAMP 10 software. Pipettes were fabricated from borosilicate glass capillaries and pulled by a P-97 instrument (Sutter Instruments, Novato, CA, USA) with 3.5–5.5 MΩ resistance. The experiments were carried out at room temperature (22–25°C). Potassium currents were low-pass filtered at 5 kHz and digitized at 50 kHz.^{43,46,47} The data were analysed using a combination of Clampfit version 10.2 (Molecular Devices, San Jose, CA, USA), and Microsoft Excel and Origin version 8.5 (Microcal Software, Northampton, MA, USA). The steady-state activation curves were fitted with the Boltzmann equation, $G/G_{\max} = (1 + \exp((V - V_{1/2})/k))^{-1}$, in which $V_{1/2}$ represents the membrane potential at half-maximal activation, and k represents the slope factor as described.⁴⁸ The BK current was normalized using wild-type BK current as reported previously.^{49,50}

The solutions used for the patch-clamp experiments were as follows:

Pipette solution (in mM): 160 MeSO₃K, 2 MgCl₂, and 10 4-(2-hydroxyethyl)-1-piperazin eethanesulfonic acid (HEPES).

Nominal 0 µM Ca²⁺ solution containing the following reagents (in mM): 160 MeSO₃K, 5 EGTA, and 10 HEPES.

1 µM Ca²⁺ solution containing the following reagents (in mM): 160 MeSO₃K, 5 EGTA, 3.25 CaCl₂, and 10 HEPES.

10 µM Ca²⁺ solution containing the following reagents (in mM): 160 MeSO₃K, 5 hydroxyethylethylenediaminetriacetic acid, 2.988 CaCl₂ and 10 HEPES.

For Mg²⁺-dependent experiments, the BK potassium current was recorded with a bath solution containing 0 or 10 mM Mg²⁺.

4.7 | Statistical analysis

Statistical analysis was carried out using a two-tailed Student's t-test for analysing two groups. Data are presented as means ± standard errors of the means. A *P*-value < .05 was considered to be statistically significant.

CONFLICT OF INTEREST

The authors declare no conflict of interest.

AUTHOR CONTRIBUTIONS

LL and QKW designed experiments; LL, HL, HX and XB performed basic experiments and data collection. DB, AVH, AFJ and E. A. P. were responsible for collection of clinical data; all authors analysed data; LL, TK and QKW drafted the manuscript; all authors did critical revision of manuscript; KT, CX and QW did project supervision.

DATA AVAILABILITY STATEMENT

We confirm that the data are presented in the manuscript and also available upon request.

ORCID

Lina Liang  <https://orcid.org/0000-0002-3537-0680>

Qing K. Wang  <https://orcid.org/0000-0002-2235-6572>

REFERENCES

- Brayden JE, Nelson MT. Regulation of arterial tone by activation of calcium-dependent potassium channels. *Science*. 1992;256(5056):532-535.
- Robitaille R, Charlton MP. Presynaptic calcium signals and transmitter release are modulated by calcium-activated potassium channels. *J Neurosci*. 1992;12(1):297-305.
- Wu YC, Art JJ, Goodman MB, Fettiplace R. A kinetic description of the calcium-activated potassium channel and its application to electrical tuning of hair cells. *Prog Biophys Mol Biol*. 1995;63(2):131-158.
- Montgomery JR, Meredith AL. Genetic activation of BK currents in vivo generates bidirectional effects on neuronal excitability. *Proc Natl Acad Sci U S A*. 2012;109(46):18997-19002.
- Robitaille R, Garcia ML, Kaczorowski GJ, Charlton MP. Functional colocalization of calcium and calcium-gated potassium channels in control of transmitter release. *Neuron*. 1993;11(4):645-655.
- Yuan P, Leonetti MD, Pico AR, Hsiung Y, MacKinnon R. Structure of the human BK channel Ca^{2+} -activation apparatus at 3.0 Å resolution. *Science*. 2010;329(5988):182-186.
- Jiang Y, Lee A, Chen J, Cadene M, Chait BT, MacKinnon R. Crystal structure and mechanism of a calcium-gated potassium channel. *Nature*. 2002;417(6888):515-522.
- Bao L, Rapin AM, Holmstrand EC, Cox DH. Elimination of the BK(Ca) channel's high-affinity Ca^{2+} sensitivity. *J Gen Physiol*. 2002;120(2):173-189.
- Bao L, Kaldany C, Holmstrand EC, Cox DH. Mapping the BKCa channel's "Ca²⁺ bowl": side-chains essential for Ca²⁺ sensing. *J Gen Physiol*. 2004;123(5):475-489.
- Schreiber M, Yuan A, Salkoff L. Transplantable sites confer calcium sensitivity to BK channels. *Nat Neurosci*. 1999;2(5):416-421.
- Du W, Bautista JF, Yang H, et al. Calcium-sensitive potassium channelopathy in human epilepsy and paroxysmal movement disorder. *Nat Genet*. 2005;37(7):733-738.
- Li X, Poschmann S, Chen Q, et al. De novo BK channel variant causes epilepsy by affecting voltage gating but not Ca^{2+} sensitivity. *Eur J Hum Genet*. 2018;26(2):220-229.
- Liang L, Li X, Moutton S, et al. De novo loss-of-function KCNMA1 variants are associated with a new multiple malformation syndrome and a broad spectrum of developmental and neurological phenotypes. *Hum Mol Genet*. 2019;28(17):2937-2951.
- Mameli C, Cazzola R, Spaccini L, et al. Neonatal diabetes in patients affected by Liang-Wang syndrome carrying KCNMA1 variant p.(Gly375Arg) suggest a potential role of Ca^{2+} and voltage-activated K⁺ channel activity in human insulin secretion. *Curr Issues Mol Biol*. 2021;43(2):1036-1042.
- Tabarki B, AlMajhad N, AlHashem A, Shaheen R, Alkuraya FS. Homozygous KCNMA1 mutation as a cause of cerebellar atrophy, developmental delay and seizures. *Hum Genet*. 2016;135(11):1295-1298.
- Yeşil G, Aralaşmak A, Akyüz E, İçağasioğlu D, Uygur Şahin T, Bayram Y. Expanding the phenotype of homozygous KCNMA1 mutations; dyskinesia, epilepsy, intellectual disability, cerebellar and corticospinal tract atrophy. *Balkan Med J*. 2018;35(4):336-339.
- Bailey CS, Moldenhauer HJ, Park SM, Keros S, Meredith AL. KCNMA1-linked channelopathy. *J Gen Physiol*. 2019;151(10):1173-1189.
- Zhang G, Gibson RA, McDonald M, et al. A gain-of-function mutation in KCNMA1 causes dystonia spells controlled with stimulant therapy. *Mov Disord*. 2020;35(10):1868-1873.
- Rodrigues Bento J, Feben C, Kempers M, et al. Two novel presentations of KCNMA1-related pathology—expanding the clinical phenotype of a rare channelopathy. *Mol Genet Genomic Med*. 2021;9(10):e1797.
- Graber D, Imagawa E, Miyake N, et al. Polymicrogyria in a child with KCNMA1-related channelopathy. *Brain Dev*. 2022;44(2):173-177.
- Richards S, Aziz N, Bale S, et al. Standards and guidelines for the interpretation of sequence variants: a joint consensus recommendation of the American College of Medical Genetics and Genomics and the Association for Molecular Pathology. *Genet Med*. 2015;17(5):405-424.
- Yang H, Shi J, Zhang G, Yang J, Delaloye K, Cui J. Activation of Slo1 BK channels by Mg^{2+} coordinated between the voltage sensor and RCK1 domains. *Nat Struct Mol Biol*. 2008;15(11):1152-1159.
- Chakrabarti S, Wu X, Yang Z, et al. MOG1 rescues defective trafficking of $\text{Na}_v1.5$ mutations in Brugada syndrome and sick sinus syndrome. *Circ Arrhythm Electrophysiol*. 2013;6(2):392-401.
- Xiong H, Bai X, Quan Z, et al. Mechanistic insights into the interaction of cardiac sodium channel $\text{Na}_v1.5$ with MOG1 and a new molecular mechanism for Brugada syndrome. *Heart Rhythm*. 2021. doi:10.1016/j.hrthm.2021.11.026
- Kim H-J, Lim H-H, Rho S-H, et al. Modulation of the conductance-voltage relationship of the BK_{Ca} channel by mutations at the putative flexible interface between two RCK domains. *Biophys J*. 2008;94(2):446-456.
- Xia XM, Zeng X, Lingle CJ. Multiple regulatory sites in large-conductance calcium-activated potassium channels. *Nature*. 2002;418(6900):880-884.
- Du X, Carvalho-de-Souza JL, Wei C, et al. Loss-of-function BK channel mutation causes impaired mitochondria and progressive cerebellar ataxia. *Proc Natl Acad Sci U S A*. 2020;117(11):6023-6034.
- Emrah Y, Beyza G, Cemil O, et al. Functional Characterization of KCNMA1 mutation associated with dyskinesia, seizure, developmental delay, and cerebellar atrophy. *Res Sq*. 2021.

29. Koval OM, Fan Y, Rothberg BS. A role for the S0 transmembrane segment in voltage-dependent gating of BK channels. *J Gen Physiol.* 2007;129(3):209-220.
30. Wallner M, Meera P, Toro L. Determinant for beta-subunit regulation in high-conductance voltage-activated and Ca²⁺-sensitive K⁺ channels: an additional transmembrane region at the N terminus. *Proc Natl Acad Sci U S A.* 1996;93(25):14922-14927.
31. Jeffries O, Geiger N, Rowe ICM, et al. Palmitoylation of the S0-S1 linker regulates cell surface expression of voltage- and calcium-activated potassium BK channels. *J Biol Chem.* 2010;285(43):33307-33314.
32. Duncan PJ, Bi D, McClafferty H, Chen L, Tian L, Shipston MJ. S-Acylation controls functional coupling of BK channel pore-forming α -subunits and β 1-subunits. *J Biol Chem.* 2019;294(32):12066-12076.
33. Shi P, Li D, Lai C, Zhang L, Tian C. Intracellular segment between transmembrane helices S0 and S1 of BK channel α subunit contains two amphipathic helices connected by a flexible loop. *Biochem Biophys Res Commun.* 2013;437(3):408-412.
34. Suzuki Y, Ohya S, Yamamura H, Giles WR, Imaizumi Y. A new splice variant of large conductance Ca²⁺-activated K⁺ (BK) channel α subunit alters human chondrocyte function. *J Biol Chem.* 2016;291(46):24247-24260.
35. Laumonnier F, Roger S, Guérin P, et al. Association of a functional deficit of the BK_{Ca} channel, a synaptic regulator of neuronal excitability, with autism and mental retardation. *Am J Psychiatry.* 2006;163(9):1622-1629.
36. Plante AE, Lai MH, Lu J, Meredith AL. Effects of single nucleotide polymorphisms in human KCNMA1 on BK current properties. *Front Mol Neurosci.* 2019;12:285.
37. Graber D, Imagawa E, Miyake N, et al. Polymicrogyria in a child with KCNMA1-related channelopathy. *Brain Dev.* 2022;44(2):173-177.
38. Yao YU, Qu D, Jing X, et al. Molecular mechanisms of epileptic encephalopathy caused by KCNMA1 loss-of-function mutations. *Front Pharmacol.* 2021;12:775328.
39. Persson PB. Good publication practice in physiology 2019. *Acta Physiol (Oxf).* 2019;227(4):e13405.
40. Eilbeck K, Quinlan A, Yandell M. Settling the score: variant prioritization and Mendelian disease. *Nat Rev Genet.* 2017;18(10):599-612.
41. Hu Y, Bai X, Zhang C, et al. Ubiquitination-activating enzymes UBE1 and UBA6 regulate ubiquitination and expression of cardiac sodium channel Na_v1.5. *Biochem J.* 2020;477(9):1683-1700.
42. Zhang X, Chen S, Yoo S, et al. Mutation in nuclear pore component NUP155 leads to atrial fibrillation and early sudden cardiac death. *Cell.* 2008;135(6):1017-1027.
43. Huang Y, Wang Z, Liu Y, et al. alphaB-crystallin interacts with Nav1.5 and regulates ubiquitination and internalization of cell surface Na_v1.5. *J Biol Chem.* 2016;291(21):11030-11041.
44. Tang BO, Hu Y, Wang Z, et al. UBC9 regulates cardiac sodium channel Na_v1.5 ubiquitination, degradation and sodium current density. *J Mol Cell Cardiol.* 2019;129:79-91.
45. Si W, Zhou B, Xie W, et al. Angiogenic factor AGGF1 acts as a tumor suppressor by modulating p53 post-transcriptional modifications and stability via MDM2. *Cancer Lett.* 2020;497:28-40.
46. Yu G, Liu Y, Qin J, et al. Mechanistic insights into the interaction of the MOG1 protein with the cardiac sodium channel Na_v1.5 clarify the molecular basis of Brugada syndrome. *J Biol Chem.* 2018;293(47):18207-18217.
47. Wang Z, Yu G, Liu Y, et al. Small GTPases SAR1A and SAR1B regulate the trafficking of the cardiac sodium channel Na_v1.5. *Biochim Biophys Acta Mol Basis Dis.* 2018;1864(11):3672-3684.
48. Liu H-W, Hou P-P, Guo X-Y, et al. Structural basis for calcium and magnesium regulation of a large conductance calcium-activated potassium channel with β 1 subunits. *J Biol Chem.* 2014;289(24):16914-16923.
49. Sun X-H, Ding J-P, Li H, et al. Activation of large-conductance calcium-activated potassium channels by puerarin: the underlying mechanism of puerarin-mediated vasodilation. *J Pharmacol Exp Ther.* 2007;323(1):391-397.
50. Yao J, Chen X, Li H, et al. Bmp09, a "long chain" scorpion peptide blocker of BK channels. *J Biol Chem.* 2005;280(15):14819-14828.

SUPPORTING INFORMATION

Additional supporting information may be found in the online version of the article at the publisher's website.

How to cite this article: Liang L, Liu H, Bartholdi D, et al. Identification and functional analysis of two new de novo *KCNMA1* variants associated with Liang-Wang syndrome. *Acta Physiol.* 2022;235:e13800. doi:[10.1111/apha.13800](https://doi.org/10.1111/apha.13800)